Hysteresis loops at different temperatures for melt-spun $Nd_{13}Fe_{77}B_{10}$

1998 J. Phys.: Condens. Matter 10 7243

(http://iopscience.iop.org/0953-8984/10/32/015)

J. Phys.: Condens. Matter **10** (1998) 7243–7258. Printed in the UK PII: S0953-8984(98)93544-5

Hysteresis loops at different temperatures for melt-spun $Nd_{13}Fe_{77}B_{10}$

Jin Han-min†‡, Y B Kim† and Wang Xue-feng‡

† Korea Research Institute of Standards and Science, Taejon 305-606, Korea

‡ Department of Physics, Jilin University, Changchun, 130023, People's Republic of China

Received 22 April 1998

Abstract. Hysteresis loops of melt-spun $Nd_{13}Fe_{77}B_{10}$ were measured at different temperatures between 4.2 K and 250 K. The loops were analysed on the basis of the micromagnetism using the finite element technique. By fitting the calculated ${}_iH_c$ with the experiment, the value of the exchange constant across the inter-grain boundary was estimated to be about 90% of that across the inner-grain boundary. ${}_iH_c$ increases to a maximum at the spin reorientation temperature T_s and then decreases with increasing temperature. With decrease of the exchange interaction across the grain boundary, ${}_iH_c$ decreases below T_s and increases above T_s, and the Stoner–Wohlfarth model provides the theoretical lower and upper limits of ${}_iH_c$ below and above T_s, respectively. The calculations reproduce the hysteresis loops fairly well. The magnetization proceeds by non-coherent rotation, and the spin distribution becomes quite non-uniform in some grains when H decreases to near ${}_iH_c$.

1. Introduction

The melt-spun Nd–Fe–B alloys are isotropic, and the excellent permanent magnetic properties are related to the extremely fine grain structure of the tetragonal $Nd_2Fe_{14}B$ phase [1]. The $Nd_2Fe_{14}B$ has an easy axis above the spin reorientation temperature $T_s = 135$ K and an easy cone below T_s. The four easy axes are on the {110} planes, and the cone angle increases to 32 degrees with decrease of temperature to 4.2 K [2].

The grains contact each other (stoichiometric alloys [3]) or are surrounded by a very thin Nd rich phase (hyper-stoichiometric alloys [4]). The remanence J_r is larger than $J_s/2$ predicted by the Stoner–Wohlfarth (S–W) model, and for near-stoichiometric alloys J_r increases and ${}_iH_c$ decreases with decrease of the scale of the nanostructure at room temperature [1]. The phenomena are ascribed to the intergranular exchange interaction [3], which was supported by the exchange-coupled single domain model calculation [5]. Up to recent years, it had been believed that the magnetization reversal occurs by domain wall movement [4, 6] or by single domain behaviour [7]. Recently, quantitative analyses were carried out for three dimensional multi-grain magnets by using the micromagnetic finite element technique on the hysteresis loops at room temperature [8, 9] and 4.2 K [10], which show that the demagnetization proceeds by the non-coherent reversion. This work is a continuation of the previous work [10] and will analyse the temperature dependence of the hysteresis loop for the melt-spun $Nd_{13}Fe_{77}B_{10}$ magnet by using the Gaussian–Seidel method [11].

0953-8984/98/327243+16$19.50

2. Experiments

An amorphous alloy of nominal composition $Nd_{13}Fe_{77}B_{10}$ was prepared by a single wheel technique under argon atmosphere. The surface speed of the Cu wheel was 35 m s^{-1} and the alloy was 1 mm wide and ~30 μm thick. The alloy was annealed at 950 K for 10 minutes in a vacuum of 1×10^{-4} Torr. The strips were arranged into a 5 mm long, 3 mm wide, 30 μm thick rectangular shape. The specimen was cooled down to 4.2 K at remanent state after magnetization along the ribbon length direction in a pulsed field of ~7 MA m^{-1} at room temperature. The hysteresis loops were measured along the ribbon length direction at the fields of $H_{max} = 4.0$ MA m^{-1} by a high field vibrating sample magnetometer (Janis 4500/150A) at different temperatures between 4.2 K and 250 K.

3. Model and calculations

Finite and infinite magnets were analysed. The finite magnet is comprised of $3 \times 3 \times 3$ cubic $Nd_2Fe_{14}B$ grains of dimension L. Both the c- and [100]-axes of the grains are randomly oriented. Each grain is divided into $m \times m \times m$ cubic single domain elements of equal dimension. So the magnet consists of $(3 \times m)^3$ equi-dimensional cubic single domain elements. Each element is exchange coupled with the adjacent elements. The infinite magnet is built by piling up infinite number of the finite magnets, and the periodic boundary conditions hold for each sub-magnet. The total energy is the sum of the magnetocrystalline anisotropy energy G_K, the Zeeman energy G_H, the exchange energy G_X and the stray field energy G_S, where

$$G_K = \sum_i F_K(i) = \sum_i [K_1 \sin^2\theta(i) + K_2 \sin^4\theta(i) + K_3 \sin^4\theta(i) \cos(4\phi(i))] \tag{1}$$

$$G_H = \sum_i F_H(i) = -\sum_i \boldsymbol{J}_s \cdot \boldsymbol{H} \tag{2}$$

$$G_x = \frac{1}{2}\sum_i F_X(i) = \frac{1}{2}\sum_i -\frac{m}{\mu_0 L} \sum_{j=adjacent} w(i,j)\boldsymbol{J}_s(i) \cdot \boldsymbol{J}_s(j)$$
$$(i = 1, 2, \ldots, (3 \times m)^3). \tag{3}$$

Here, $\theta(i)$ and $\phi(i)$ are the polar angles of the magnetic moment vector of the ith element $\boldsymbol{J}_s(i)$ in the $\langle 100 \rangle$ coordinate system and $w(i, j)$ is the exchange constant per unit boundary area between the ith and its adjacent jth element. Let w_i denote the constant for the inner-grain boundary, w_b for the inter-grain boundary and w when it is assumed that $w_i = w_b$.

For a given applied field, the magnetization J was obtained from minimization of the total energy. The effect of the stray field is small [5, 8] while it consumes very large CPU time and was neglected for the infinite magnet. The effect was examined for the finite magnet for which the CPU time can be reduced by replacing the stray field energy by the function of

$$W = \frac{1}{2\mu_0}\int (\nabla \times \boldsymbol{A} - \boldsymbol{J}_s)^2 \, \mathrm{d}^3 r \tag{4}$$

and J could be obtained from minimization of the function of

$$G = G_K + G_H + G_X + W \tag{5}$$

with respect to $\{\theta(i), \phi(i)\}$ $(i = 1, 2, \ldots, (3 \times m)^3)$ and $\{A_x(\boldsymbol{r}), A_y(\boldsymbol{r}), A_z(\boldsymbol{r})\}$, where $A_x(\boldsymbol{r})$, for instance, is the x component of $\boldsymbol{A}$ at position $\boldsymbol{r}$ and the integration in equation (4) extends to the whole space [8, 12]. In this work, the space was limited within a cubic

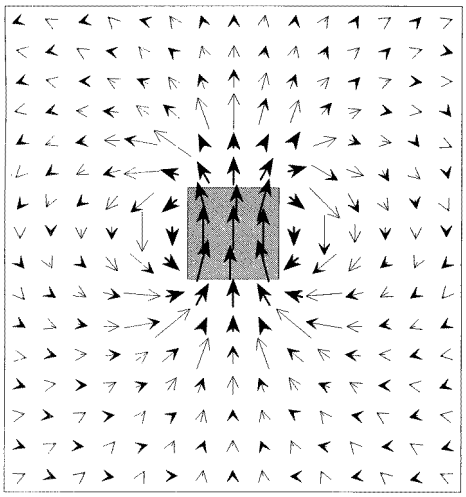

(a)

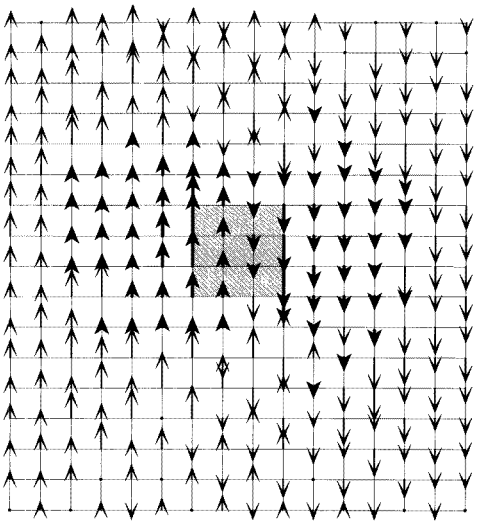

(b)

Figure 1. Distribution of $\boldsymbol{B}$ (figure a) and A_x (figure b) for the saturated finite magnet calculated with distant boundary.

boundary encircling the magnet symmetrically (figure 2(a)). The space was gridded by extending the grid made up by the edges of the cubic magnetic elements, and the integration was replaced by the summation. By allotting the variables of A_x, A_y and A_z to each grid point, and by assuming that they vary continuously in the space, $\partial A_z/\partial y$ for element (n_x, n_y, n_z) with the corners n'_x, n'_y and n'_z ($n'_x = n_x$, $n_x + 1$, $n'_y = n_y$, $n_y + 1$, $n'_z = n_z$, $n_z + 1$), for instance, is approximated as

$$\frac{\partial A_z}{\partial y} \approx \frac{1}{4} \sum_{n'_x = n_x, n_x+1} \sum_{n'_z = n_z, n_z+1} \frac{A_z(n'_x, n_y + 1, n'_z) - A_z(n'_x, n_y, n'_z)}{L/m}. \tag{6}$$

The minimization of G was carried out in respect to $\theta(i)$, $\phi(i)$ ($i = 1, 2, \ldots, (3 \times m)^3$),

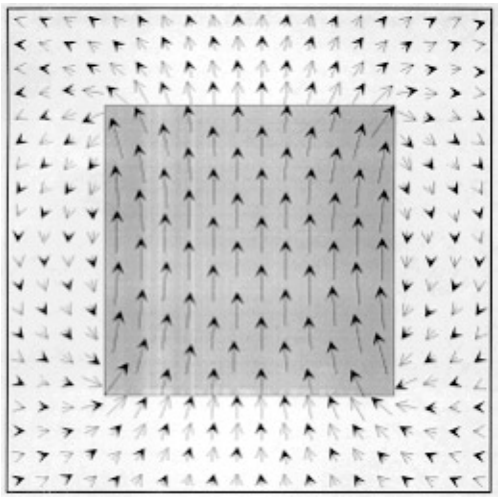

(a)

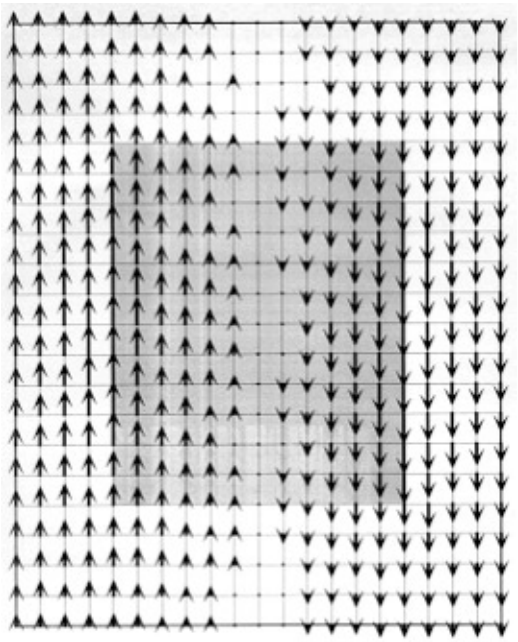

(b)

Figure 2. Distribution of $\boldsymbol{B}$ (figure a) and A_x (figure b) for the saturated finite magnet calculated with nearby boundary.

and $A_x(\alpha)$, $A_y(\alpha)$ and $A_z(\alpha)$ ($\alpha = 1, 2, \ldots$, through all grid points within the boundary) under the following boundary conditions. $\boldsymbol{A}$ on the boundary was calculated as the sum of the magnetic vector potentials produced by the magnetic dipoles of the magnetic elements, i.e.

$$\boldsymbol{A}(\alpha) = \left(\frac{L}{m}\right)^3 \sum_i \frac{\boldsymbol{J}(i) \times (\boldsymbol{r}(\alpha) - \boldsymbol{r}(i))}{4\pi |\boldsymbol{r}(\alpha) - \boldsymbol{r}(i)|} \qquad (i = 1, 2, \ldots, (3 \times m)^3) \quad (7)$$

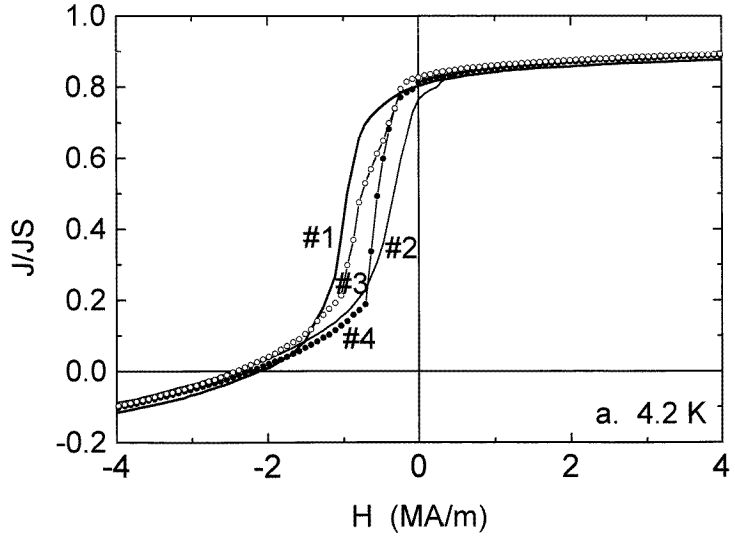

(a)

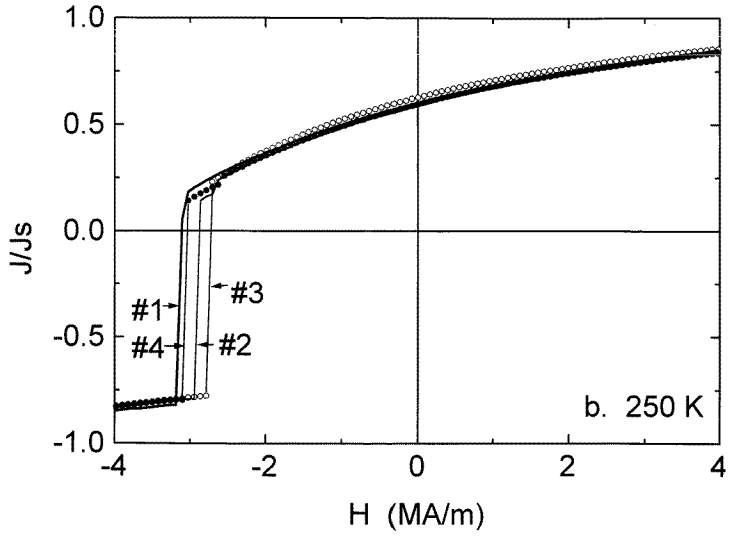

(b)

Figure 3. Part of the hysteresis loops calculated for four infinite magnets of different grain distributions. (a) 4.2 K, (b) 250 K. d$G < 0$, $m = 4$, and $w/L = 0.35$.

where $\boldsymbol{r}(\alpha)$ and $\boldsymbol{r}(i)$ are the position vectors of the grid point α on the boundary and the ith magnetic element, respectively.

Figures 1 and 2 demonstrate the space distribution of the magnetic flux density $\boldsymbol{B}$ and A_x for the magnet saturated along the z direction. The sections are parallel to the yz-plane and were cut in the middle of the magnet. The shaded area is the magnet.

In figure 1, the boundary is distant enough from the magnet that it is out of the figure and the boundary condition of $\boldsymbol{A} \approx \boldsymbol{0}$ holds. Figure 1(a) shows the $\boldsymbol{B}$ distribution. The

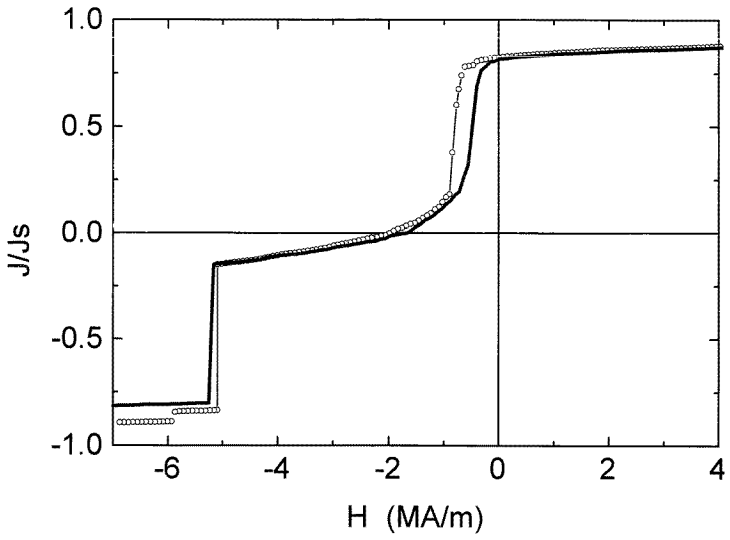

Figure 4. Part of the hysteresis loops at 4.2 K calculated for the finite magnet 1. The stray field energy is neglected for the curve without symbols and is taken into account for the curve with symbols. $dG < 0$.

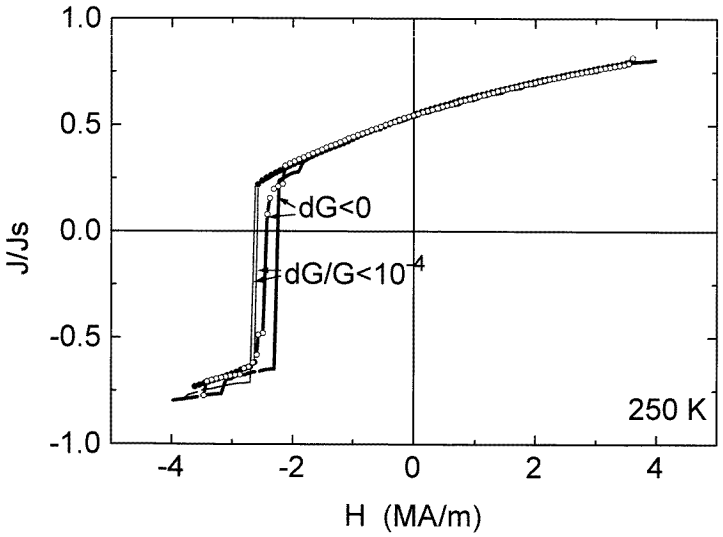

Figure 5. Part of the hysteresis loops at 250 K calculated for the finite magnet 1. The curves without symbols were calculated by neglecting the stray field energy, and the curves with symbols by taking into account the stray field energy. $dG/G < 10^{-4}$ for the thin curves and $dG < 0$ for the bold curves.

length of the thin arrows and ten times of the length of the bold arrows represents the value of $\boldsymbol{B}$. The bold arrows and the thin arrows with bold tips were calculated from the relation of

$$\boldsymbol{B} = \boldsymbol{\nabla} \times \boldsymbol{A} \tag{8}$$

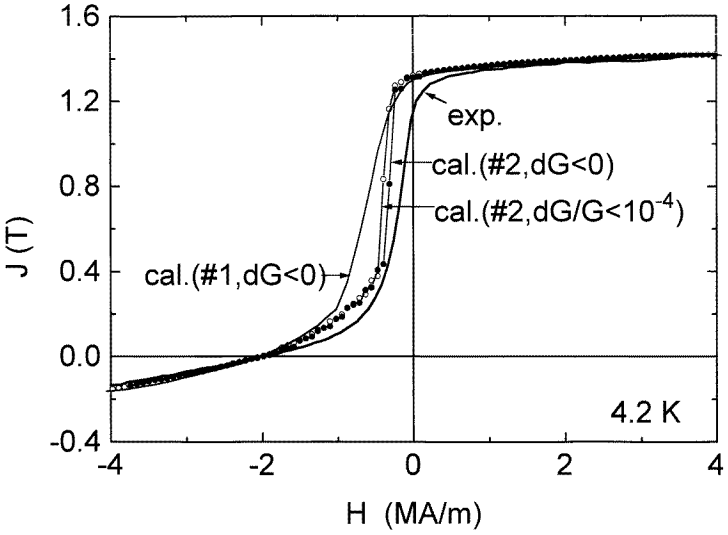

(a)

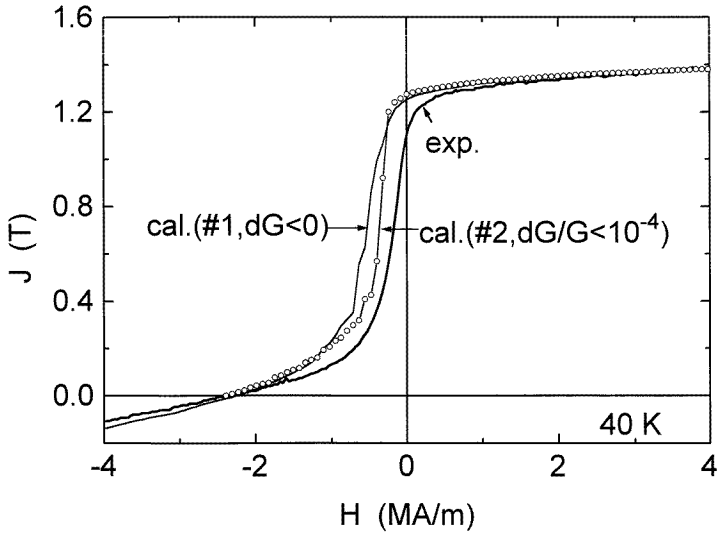

(b)

Figure 6. Part of the hysteresis loops at 4.2 K (a), 40 K (b), 100 K (c), 125 K (d), 150 K (e), 180 K (f) and 250 K (g).

by using the data of $\{A_x(\alpha), A_y(\alpha), A_z(\alpha)\}$ obtained from the minimization of W. The thin arrows with thin tips are the theoretical ones calculated from equations (7) and (8). The two calculations agree fairly well around the magnet, but disagreement is obvious in the region distant from the magnet where $\boldsymbol{B}$ is small. Figure 1(b) shows the distribution of A_x. The length of the thin arrows and ten times of the length of the bold arrows represents the absolute value of A_x. The value is positive for the upward directed arrows and is negative

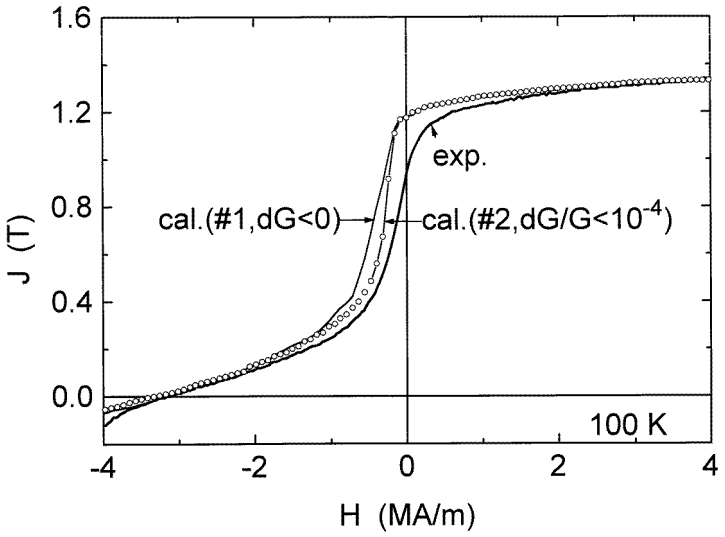

(c)

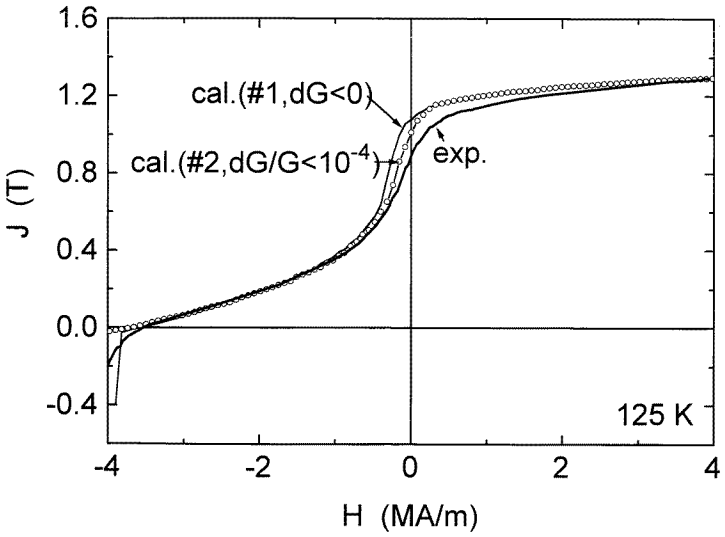

(d)

Figure 6. (Continued)

for the downward directed arrows. It can be seen that the assumption of continuous variation of A_x does not hold at some regions distant from the magnet.

A satisfactory result could be obtained for the smaller space of figure 2. The bold square in the figure represents the boundary. Figure 2(a) shows the $\boldsymbol{B}$ distribution. The result of the above mentioned method (the arrows with bold tips) coincides with the theoretical one (the arrows with thin tips) well. Figure 2(b) shows the distribution of A_x, which demonstrates that $\boldsymbol{A}$ varies continuously as was assumed. Hereafter, the boundary geometry of figure 2 will be used.

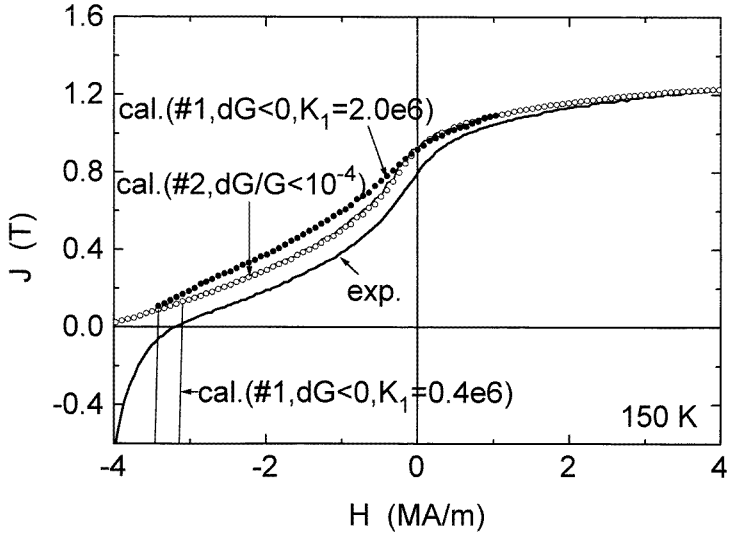

(e)

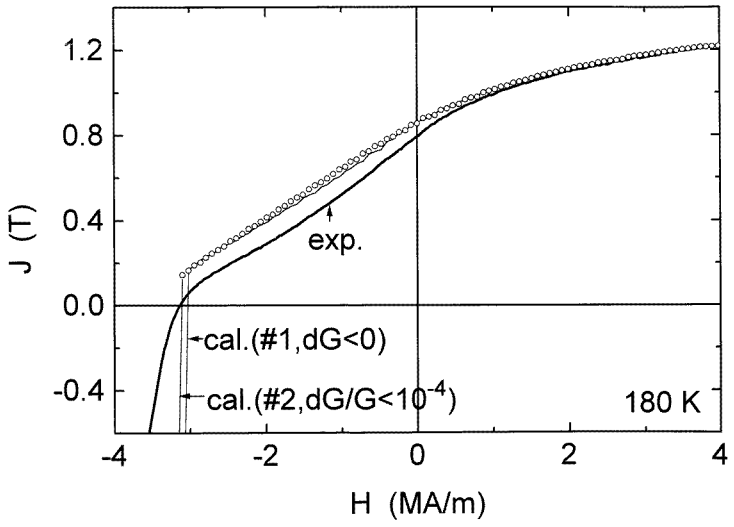

(f)

Figure 6. (Continued)

The algorithm of the minimization for a given applied field is as follows:

(1) $\{\theta(i), \phi(i)\}$ are obtained from the minimization conditions of

$$\delta G(i) = \delta[(F_K(i) + F_H(i) + F_X(i) + W(i))] > 0 \qquad (i = 1, 2, \ldots, (3 \times m)^3) \tag{9}$$

with respect to $\theta(i)$ and $\phi(i)$ as follows. The transitional angles $\theta(i)$ and $\phi(i)$ for the ith element are obtained from the minimization of $G(i)$ within $\Delta\theta(i)$ and $\Delta\phi(i) = 0, \pm d$ ($d = 2$ degrees) under fixed magnetization of the other elements. After a cycle of the computation through the $(3 \times m)^3$ elements, G is computed. G decreases with increasing

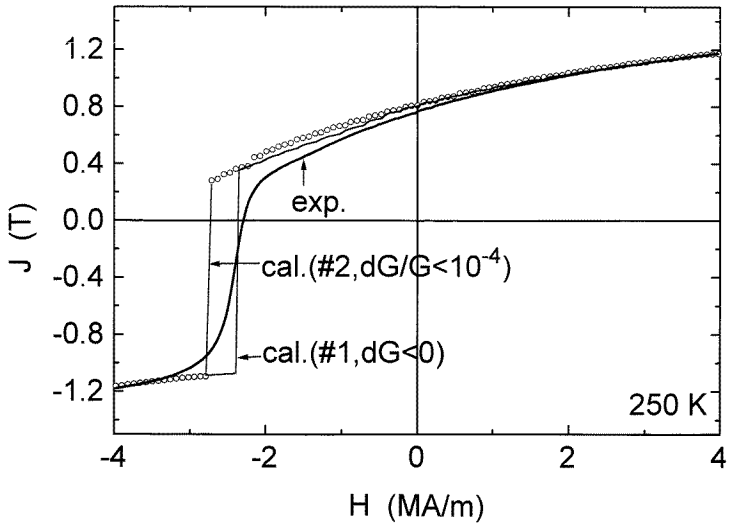

(g)

Figure 6. (Continued)

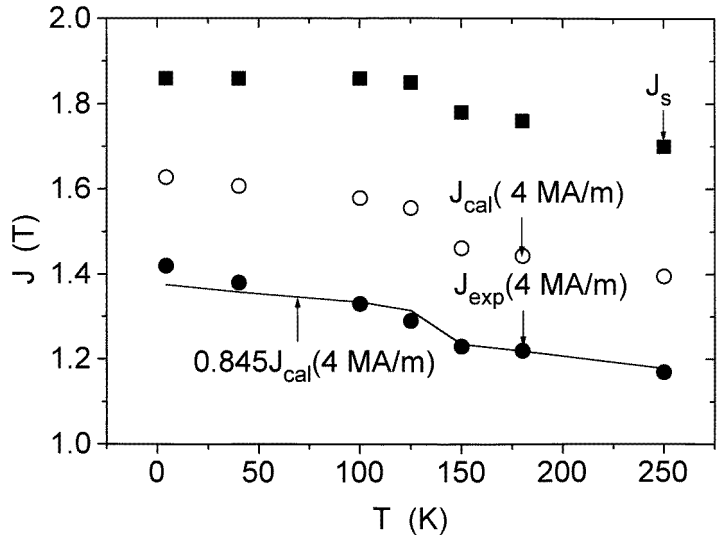

Figure 7. The temperature dependence of J_s, J_{exp}(4 MA m^{-1}), J_{calc}(4 MA m^{-1}) for magnet 1, and $0.845J_{calc}$(4 MA m^{-1}). d$G < 0$.

cycle with small fluctuation. The cycle is repeated until the minimum of G (hereafter the criterion is denoted by d$G < 0$) occurs k times. Refer to [10] for the details. The value of k was set to 10 unless otherwise mentioned. To save CPU time, the condition of the 'minimum of G' was replaced by 'the difference of G from the value of the previous cycle becomes less than 0.01%' (hereafter the criterion is denoted by d$G/G < 10^{-4}$) in some calculations.

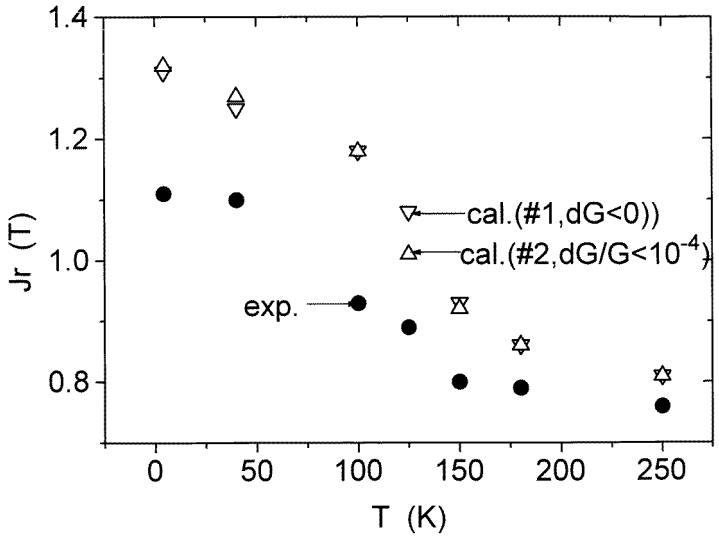

Figure 8. The temperature dependence of J_r(exp.) and J_r(calc.) for magnets 1 ($dG < 0$) and 2 ($dG/G < 10^{-4}$).

(2) $\{A_x(\alpha), A_y(\alpha), A_z(\alpha)\}$ are obtained from the minimization conditions of

$$\delta W(\alpha) > 0 \qquad (\alpha = 1, 2, \ldots \text{ through all elements in the encircled space}) \tag{10}$$

with respect to $A_x(\alpha)$, $A_y(\alpha)$ and $A_z(\alpha)$ with $k = 1$. Here $W(\alpha)$ is the terms of W which include the variables $A_x(\alpha)$, $A_y(\alpha)$ and $A_z(\alpha)$.

The demagnetization field was approximated by $-J/3\mu_0$. The values of $J_s(t)$ were taken from [13] and $K_1(T)$, $K_2(T)$ and $K_3(T)$ from [14], and are listed in table 1. The values of w_i/L and w_b/L were obtained by fitting the calculated ${}_iH_c$ for the infinite magnet to the experimental values at 4.2 K and 250 K. The value of m was set to 17 unless mentioned otherwise.

Table 1. The values of J_s, K_1, K_2 and K_3.

T (K)	J_s [13] (T)	(10^6 J m^{-3}) K_1	K_2	K_3 [14]
4	1.86	−16	27	0.45
40	1.86	−14	26	0.38
100	1.86	−8	21	0.24
125	1.85	−4.4	17	0.15
150	1.78	0.4	14.4	0
180	1.76	4	4.7	0
250	1.70	6	1	0

4. Results and discussion

Figure 3 shows part of the hysteresis loops at 4.2 K (figure a) and 250 K (figure b) calculated for four infinite magnets of different grain distributions, 1–4. It can be seen that the difference in grain distribution affects the step regions but has little effect on the other parts.

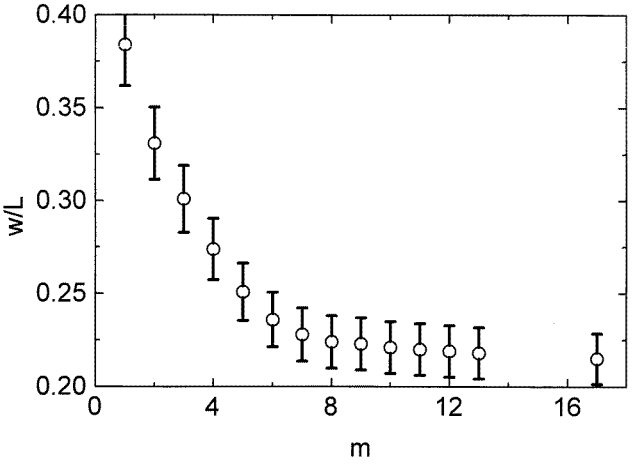

Figure 9. m dependence of w/L.

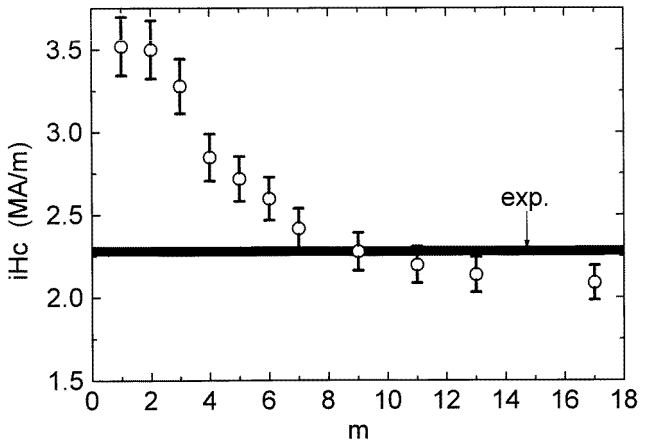

Figure 10. m dependence of ${}_iH_c$ at 250 K.

Figure 4 compares part of the hysteresis loops at 4.2 K calculated for the finite magnet 1 by neglecting and by taking into account the stray field energy. It can be seen that the stray field energy affects the loop little except that it shifts the low field step leftward apparently.

Figure 5 shows similar loops at 250 K. One set of the curves was calculated for $\mathrm{d}G/G < 10^{-4}$, and the other set for $\mathrm{d}G < 0$. The looser criterion of $\mathrm{d}G/G < 10^{-4}$ results in somewhat larger ${}_iH_c$, and the stray field has little effect except that it shifts the step a bit.

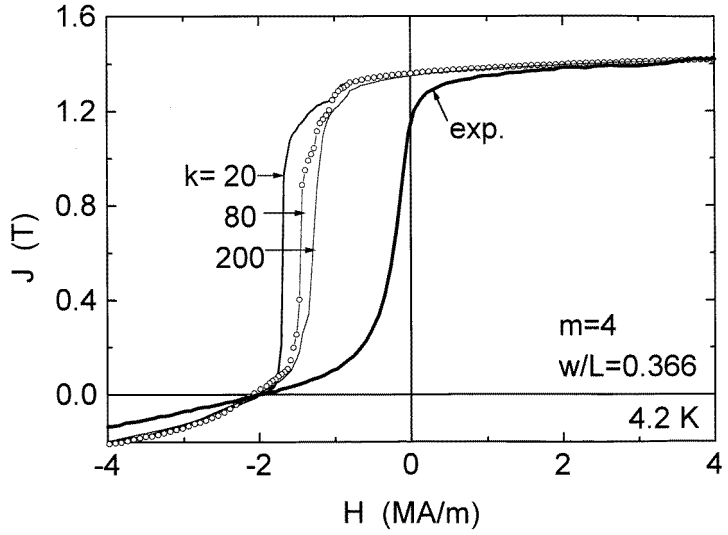

Figure 11. Hysteresis loops at 4.2 K calculated for $k = 20$, 80 and 200 ($m = 4$, $w/L = 0.366$).

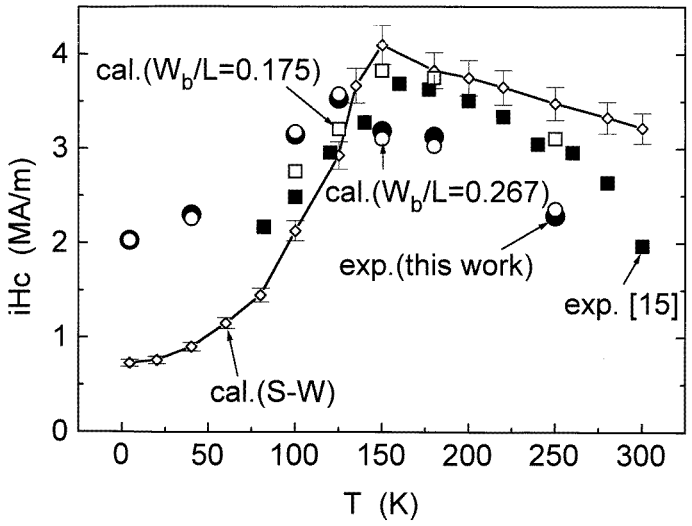

Figure 12. Temperature dependence of ${}_iH_c$.

Figure 6 shows part of the hysteresis loops of experiment and calculation at 4.2 K (a), 40 K (b), 100 K (c), 125 K (d), 150 K (e), 180 K (f) and 250 K (g). The calculations are for the infinite magnet 1 ($\mathrm{d}G < 0$) and for the magnet 2 ($\mathrm{d}G/G < 10^{-4}$). The calculation for the magnet 2 for $\mathrm{d}G < 0$ is also presented for reference in figure 6(a). The values of $w_i/L = 0.294$ and $w_b/L = 0.267$ were obtained for magnet 1 and the values of $w_i/L = 0.294$ and $w_b/L = 0.255$ were used for magnet 2. In figure 6(e) ($T = 150$ K), the loop for magnet 1 calculated with $K_1 = 2.0 \times 10^6$ J m^{-3} is presented along with that with $K_1 = 0.4 \times 10^6$ J m^{-3} (table 1), which demonstrates that the error in the values of the intrinsic magnetic parameters does not affect the loop very sensitively. Figure 7 is obtained from

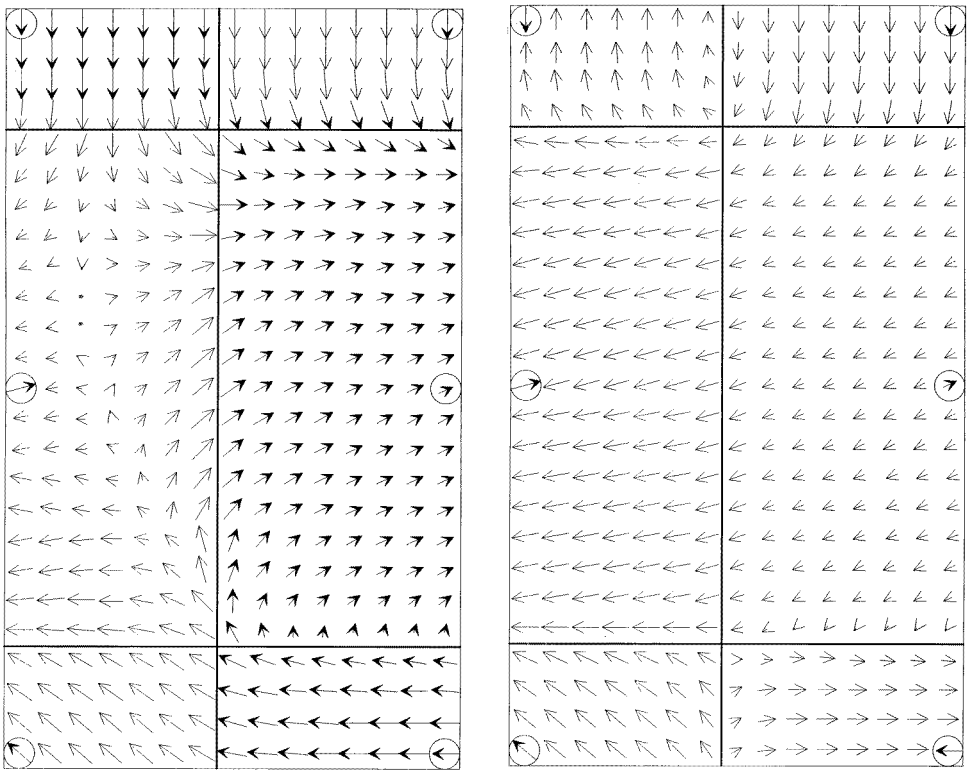

(a) (b)

Figure 13. The $J_s(r)/J_s$ distribution at the state of $J/J_s = 0.28$ (figure a) and $= -0.74$ (figure b) for infinite magnet 1 at 250 K.

table 1 and the above figures and shows the temperature dependences of J_s, $J(4\ \mathrm{MA\ m^{-1}})$ of the experiment and calculation for magnet 1, and the calculated $J(4\ \mathrm{MA\ m^{-1}})$ multiplied by 0.845. The latter curve coincides with the experiment well showing that about 15% non-magnetic minor phases are included in the alloy. The calculated curves in figure 6 are the 0.845 times the calculations. It can be seen that with increase of temperature, the high field step shifts rightwards, while the low field step shifts oppositely becoming less steep and disappears finally at around 200 K apparently higher than T_s. The last result shows that the low field step is not uniquely attributable to the cone anisotropy [10]. It also appears in the case of axial anisotropy if K_1 is smaller than K_2. The calculations reproduce the experiment fairly well except that the calculated magnetizations are larger than the experiment at and near the low field step. Figure 8 shows the temperature dependences of J_r both of the experiment and calculations. The J_r of the calculations do not depend on the grain distribution sensitively, and are apparently larger than the experiment. The discrepancy of the calculations from experiment is caused in part by not enough large value of m. Figure 9 shows the m dependence of w/L. The value of w/L for each m was obtained from fit of the calculated ${}_iH_c$ with the experiment at 4.2 K. Figure 10 shows the m dependences of ${}_iH_c$ at 250 K calculated with the values of w/L. It can be seen that $m = 17$ is not large enough to decrease the values of w/L and ${}_iH_c$ to the limits. Figure 10 of [10] shows that the increase of m improves the simulation of the low field step apparently. The

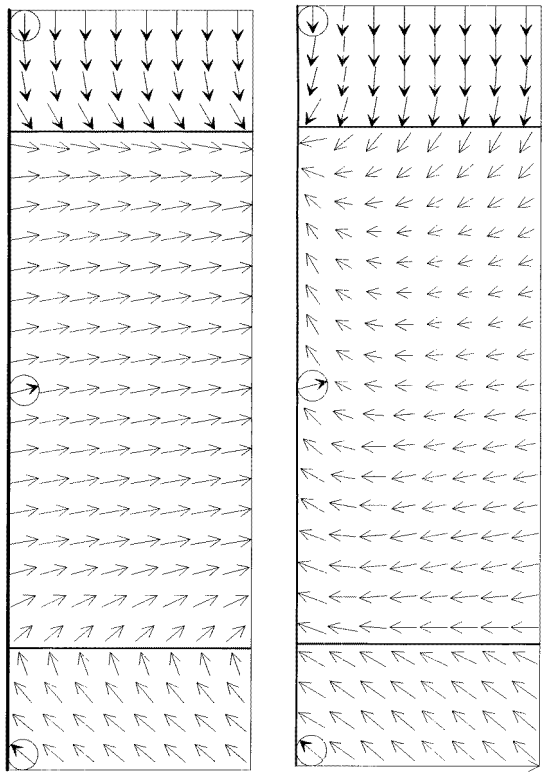

(a) (b)

Figure 14. The $\boldsymbol{J}_s(\boldsymbol{r})/J_s$ distribution at the state of $J/J_s = 0.25$ for finite magnet 1 (figure a) and at the state of $J/J_s = 0.28$ for infinite magnet 1 (figure b) at 250 K.

not sufficiently large value of k also attributes to the discrepancy partly as is demonstrated in figure 11. Further increase of m and k in practice, however, is not practicable because of unbearable increase of the CPU time. It is thought that more important cause of the discrepancy is the neglect of the minor phases, including pure iron, in our model. The steep decrease of magnetization at the steps, which is another discrepancy of the calculation from the experiment, could be improved if the grain size distribution was taken into account [10].

Figure 12 shows the temperature dependence of ${}_iH_c$ both of experiment and calculation. The experimental result of Hilscher [15] is also presented. The calculations for magnet 1 coincide with the experiment very well. The calculations with the same value of w_i/L and smaller value of $w_b/L = 0.175$ result in smaller ${}_iH_c$ below T_s and larger ${}_iH_c$ above T_s, and simulate the experiment of Hilscher *et al* well. It is notable that the S–W model ($w_i/L = \infty$, $w_b/L = 0$) provides the theoretical lower limit of ${}_iH_c$ below T_s, while it presents the upper limit above T_s as known. The good reproduction of ${}_iH_c$ and poor simulation of J_r in this work is in contrast to the poor reproduction of ${}_iH_c$ and good simulation of the J_r reported in [8] and [9].

Figures 13(a) and 13(b) show the spin distributions at a part of six grains of infinite magnet 1 at 250 K just before the irreversible rotation occurs ($J/J_s = 0.28$) and after the irreversible reversal ($J/J_s = -0.74$). The section was cut at the middle of the magnet parallel to the magnet surface which is perpendicular to the applied field. The bold lines

represent the grain boundaries. The arrows inside the circles are the unit easy direction vectors and those outside the circles the unit magnetization vectors. The length of an arrow represent the projection on the section. The bold and thin arrows denote that the projection of the vector onto the positive field direction is positive and negative, respectively. The diameter of a circle represents the magnitude of a unit vector. It can be seen that the transition of magnetization from one grain to a neighbouring one is fairly smooth, and the magnetizations of the grains are strongly interdependent.

Figure 14(a) shows the spin distribution in the grains adjacent to a surface of finite magnet 1 at the state of $J/J_s = 0.25$. The boldest line represents the surface. Figure 14(b) shows the distribution in the same grains in infinite magnet 1 at the state of $J/J_s = 0.28$. While the hysteresis loops are nearly the same for the finite and infinite magnets (figure 5 and 6(g)), the spin distribution is apparently different. The difference is expected because the exchange coupling conditions are different at the magnet and sub-magnet surfaces.

In summary, the magnetic hysteresis loops for the nanocrystalline $Nd_{13}Fe_{77}B_{10}$ magnet at different temperatures can be explained fairly well quantitatively by assuming that the magnetic properties of the grains are uniform. The S–W model presents the lower and upper theoretical limits of ${}_iH_c$ below T_s and above T_s, respectively. The hysteresis loops calculated for the finite and infinite magnets are essentially the same, but the spin distribution is fairly different. The spin distribution becomes very non-uniform in some grains when the field decreases to near $-{}_iH_c$.

Acknowledgments

This work was supported by the Ministry of Science and Technology of Korea and the National Science Foundation of China.

References

[1] Manaf A, Buckley R A, Davies H A and Leonowicz M 1991 *J. Magn. Magn. Mater.* **101** 360
[2] Cadogan J M, Gavigan J P, Givord D and Li H S 1988 *J. Phys. F: Met. Phys.* **18** 779
[3] Clemente G B, Keem J E and Bradley J P 1988 *J. Appl. Phys.* **64** 5299
[4] Mishra R K 1986 *J. Magn. Magn. Mater.* **54–57** 450
[5] Fukunaga H and Inoue H 1992 *Japan. J. Appl. Phys.* **31** 1347
[6] Pinkerton F E and Fuerst C D 1990 *J. Appl. Phys.* **67** 4753
[7] Croat J J, Herbst J F, Lee R W and Pinkerton F E 1984 *J. Appl. Phys.* **55** 2078
[8] Fischer R, Schrefl T, Kronmuller H and Fidler J 1996 *J. Magn. Magn. Mater.* **153** 35
[9] Kronmuller H, Fisher R, Seeger M and Zern A 1996 *J. Phys. D: Appl. Phys.* **29** 2274
[10] Han-min Jin, Kim Y B, Park W S, Park M J and Wang Xue-feng 1998 *J. Phys.: Condens. Matter* **10** 389
[11] Torre E D 1986 *IEEE Trans. Magn.* **MAG-22** 484
[12] Asselin P and Thiele A A 1986 *IEEE Trans. Magn.* **MAG-22** 1876
[13] Hirosawa S, Matsuura Y, Yamamoto H, Fujumura S, Sagawa M and Yamauchi M 1986 *J. Appl. Phys.* **59** 873
[14] Sagawa M, Hirosawa S, Yamamoto H, Fujimura S and Matsuura Y 1987 *Japan. J. Appl. Phys.* **26** 785
[15] Hilscher G, Grossinger R, Heisz S, Sassik H and Wiesiinger G 1986 *J. Magn. Magn. Mater.* **54–57** 577